Structural performance assessment of post-tensioned concrete beams by embedded continuous fibre optics

Structural performance assessment of post-tensioned concrete beams by embedded continuous fibre optics

Daniel Ekström

WSP Sweden AB, Gothenburg, Sweden

Rasmus Rempling, Ignasi Fernandez

Chalmers University of Technology, Gothenburg, Sweden

Carlos Gil

Thomas Concrete, Gothenburg, Sweden

ABSTRACT

Prestressed concrete structures have numerous advantages over conventionally reinforced concrete, though the usage of post-tensioned structures has declined over the last two decades. By distributed optical fibre sensors, key performance indicators of the post-tensioned concrete specimens were monitored and evaluated. Initial losses and long-term effects affecting prestressing force, deflections and cracks were tracked and compared to theoretical calculation methods. It was found that the theoretical calculation methods mostly agreed well with results from the distributed optic fibre sensors. The loss of prestressing force due to mechanical creep and relaxation was overestimated in theoretical calculation methods by approximately 6 %, while the loss due to friction was overestimated by 0.6 %. Regarding deflections, the relative error ranged from 0 % to 3.3 % and 0 % to 2.9 % for the reference specimen and post-tensioned beam respectively.

Keywords: Post-tensioned concrete, Distributed optical fibre sensing, Prestressing force, Rayleigh backscattering, Crack monitoring, Performance indicators.

1 Introduction

In the beginning of the 1900th century usage of concrete structures was commonly connected with issues as creep and shrinkage. These effects were not well understood at this time [1] and to solve these issues and delay cracking of the concrete, development of prestressed concrete structures started to take place. Even though there are several benefits using post-tensioning [2,3], in later years the usage of this type of system in concrete bridges has decreased, see Figure 1. There are several possible explanations for this development, such as the complexity during construction and longer construction time, as well as difficulties to perform structural assessments on old bridges. To be able to determine the functionality and safety of these structures, information about the residual prestressing force in the tendons after time is needed which still is limited to achieve.

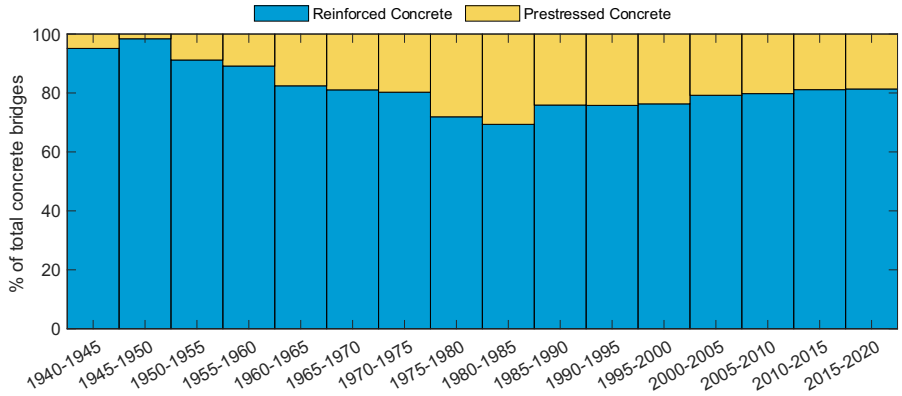

Figure 1. Reinforcement technology used in the concrete bridges built in Sweden

2 Purpose and aim

The purpose of this study was to investigate the usability of fibre optics to monitor the performance of post-tensioned concrete beams. The following objectives defined the purpose:

- Assess suitable performance indicators during the initial relaxation shrinkage and creep of the beam.
- Assess distributed optic fibre sensors as a mean to monitor the structural performance of a post-tensioned beam.

3 Method

The scientific approach included several steps. First, distributed optical fibre sensors (DOFS) was evaluated and critically selected. Second, a design and analysis of the experimental specimens including the deployment of the DOFS were assessed and performed. And, finally, the post-processing of data and material tests concluded the experimental work. In this section, each of these steps are explained further.

3.1 Optical fibre sensors

In the last decades, researchers have found out that Optic fibre sensors (OFS) of different types can be used to measure the behaviour of structures in real-time [5,6]. OFS has shown several benefits such as a high durability, low weight, good stability, and good resistance against both corrosion, chemicals, and electromagnetic fields [8]. There are several types of OFS and measuring techniques and they all have different benefits and drawbacks. The main drawbacks with one of the most common technique, Fibre Bragg grating (FBG) is the limitation of numbers of measuring points along the fibre length. This could result in uncertainties of the actual health of a structure since data of critical sections could fall out of the measuring scope [7]. In later years researchers has developed DOFS, which take advantage of the full fibre length and gives a spatial resolution and accuracy incomparable to the older developed systems with point measuring. The type used in this study was DOFS.

3.2 Design and analysis of experiments

The design of the specimens was made according to EuroCode 2 [8] for bending, shear and anchoring capacity. The cross-section geometry was decided to be made as an I-section, with flanges at top and bottom, and a web. The final design of the beams is presented in Figure 2. The properties of the materials and the dimensions of the reinforcement as well as the duct are presented in Table 1. The used post-tensioning system was an XF Live-end anchorage, consisting of XF20 anchorage system and a roll-formed flat metal duct.

3.3 Deployment of distributed optical fibre sensors

The DOFS used in this experiment were a robust type from Solifos named BRUsens V9, with an outer diameter of 3.2mm. Fibre optic strain sensing cable, mini, flexible, armoured with

central metal tube and covered with structured PA outer sheath. Strain range up to 1% (10000 µstrain). To reduce the risk of rupturing during installation this fibre suits well due to its high durability and strength. The DOFS was strategically placed along longitudinal reinforcement in both beams before casting, as seen in Figure 2. The optical fibre wire was placed back and forth in the beams. To decrease the usage of fibre, the reference beam was only equipped with fibre in the horizontal centre of the beam in in three layers (mid, top and bottom). The DOFS were bonded to the reinforcement using electrical tape. After the installation was made and the fibres were connected to the measuring unit, the fibres were pinched at specific points at the ends of the beams to locate the position of start and end points of the fibres. Four separated channels were used in total with three from the PRC beam and one from the RC beam.

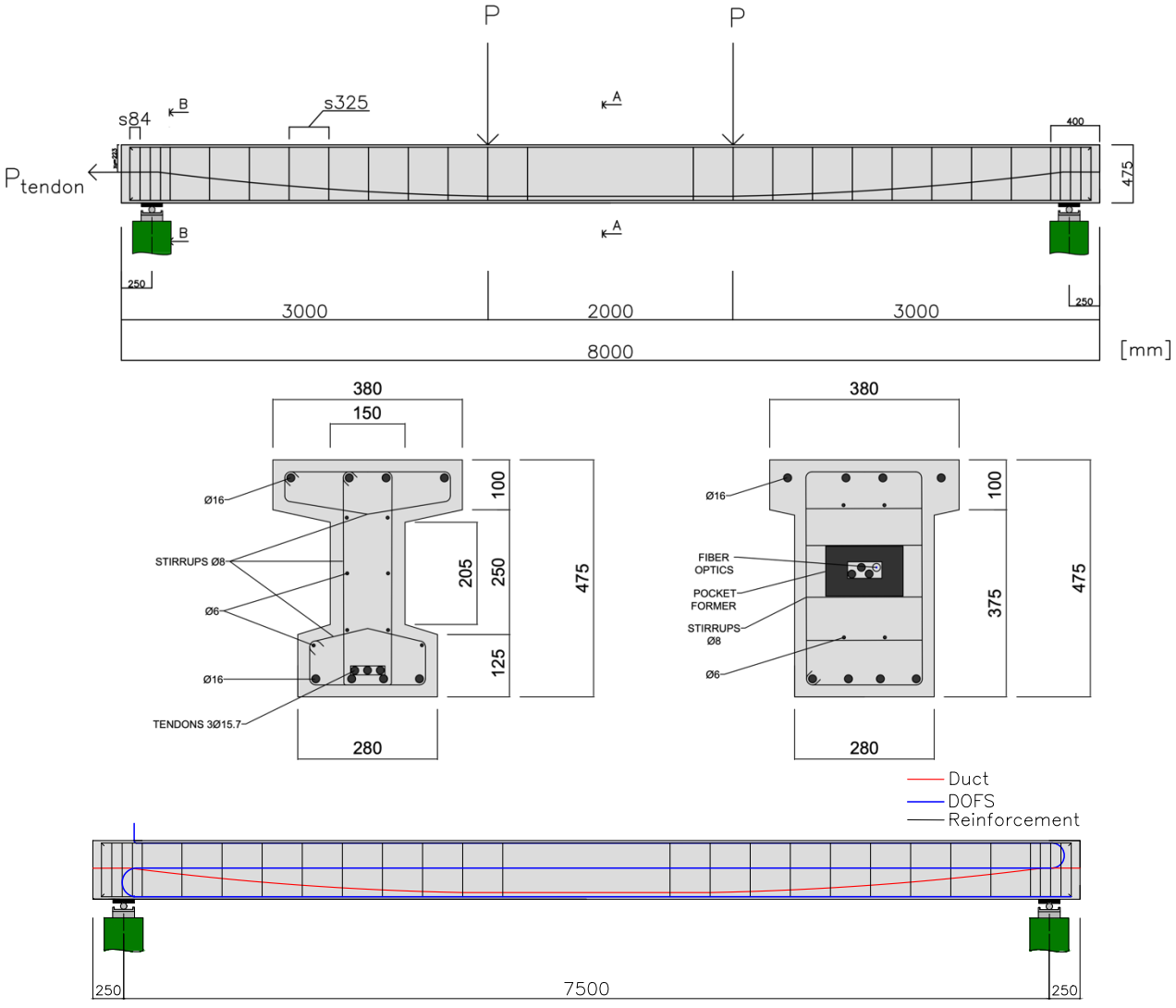

Figure 2 (Upper and middle figure) The design of the specimens was made according to EuroCode 2 for bending, shear and anchoring capacity. The cross-section geometry was decided to be made as an I-section, with flanges at top and bottom, and a web (Lower figure) The DOFS was strategically placed along longitudinal reinforcement in both beams before casting.

Table 1 Material properties and the dimensions of the reinforcement and duct

Concrete properties	
Concrete class	C50/60
Cement	CEM II/A-LL 42,5R
D_{max}	16 mm
f_{cm}	65.6 MPa
Standard deviation, σ	2.44 MPa

Tensioning steel properties	
Steel designation	Y1860S7
Nominal diameter	15.7 mm
Tensile Strength, f_{puk}	1860 MPa
Steel area, A_{pi}	150 mm

Duct dimensions	
Inner duct height	18 mm
Inner duct width	69 mm
Duct wall thickness	4 mm
Duct area	1174 mm^2

Reinforcement steel dimensions and type	
Diameter	6, 8, 16 mm
Type	K500C-T

3.4 Material testing

In order to ensure the correct concrete properties, concrete cube tests were performed at two different occasions. The first test was performed approximately 28 days after casting and the second one at 63 days after casting. The five test cubes were casted at the same occasion as the beams and were after hardening stored in a water tank. The dimension of the cubes was 150x150x150 mm and the testing followed the protocol according to European Standard [8]. At the first test, two of the cubes were tested and at the second occasion the remaining three. The cylinder compressive strength for the concrete could be calculated from the cube test according to [8]. The standard deviation for the 28-day test was 1.19 MPa and 1.76 for the 64-day test

The reinforcement used in the specimens were tested for yield strength and E-modulus. The test was conducted with five test samples of each rebar size, φ6 mm, φ8 mm, and φ16 mm, respectively. The bars were tested in a tensile test and pulled until failure. The test specimens had a length of 400 mm and the distance between the clamps in the testing machine were 293 mm for the smaller dimensions of reinforcement and 254 mm for the φ16 mm bars. The average properties for the reinforcement were: E_s 189, 167, 176 GPa; f_y 566, 500, 528 MPa; and 642, 660, 633 MPa for the reinforcement diameters 6, 8 and 16, respectively.

4 Results and discussion

In the initial phase, results are presented around the time where the post-tensioning was performed. In Figure 3, the calculated deflection and curvature directly after post-tensioning is presented. The resulting strain curves are according to common assumptions. The prestressing force causes an axial force in the whole specimen, meaning that where the curvature is zero, i.e. where εtop≈εbottom, there is still a compressive strain. For the top fibre, due to the post-tensioning, tension was registered in the middle section of the length of the beam. There is some difference between the right and left fibre, which might be an effect of some rotation when tensioning the steel, but overall, the alignment is accurate. For the middle fibre, the ideal result would be a constant curve, but the tendency indicates a slightly parabolic shape, meaning that the true natural layer might be closer to the top edge of the specimen than expected.

Looking at a small-time interval during the tensioning procedure of the PRC specimen, an interesting phenomenon can be traced. As seen in Figure 4, where outside-duct strains and bottom-fibre strains are described over time for the middle section, the concrete behaviour from anchor slip can be observed. Obviously, the effect from anchor slip will differ between the active and passive prestressing edges. By tracing the response in the middle section, a mean value of the anchor slip is

captured. This strain set-back is not the same as in the prestressing steel, because at this stage the prestressing steel is not grouted, i.e. no bond, and the prestressing steel moves freely in relation to the specimen between the anchorages at both sides.

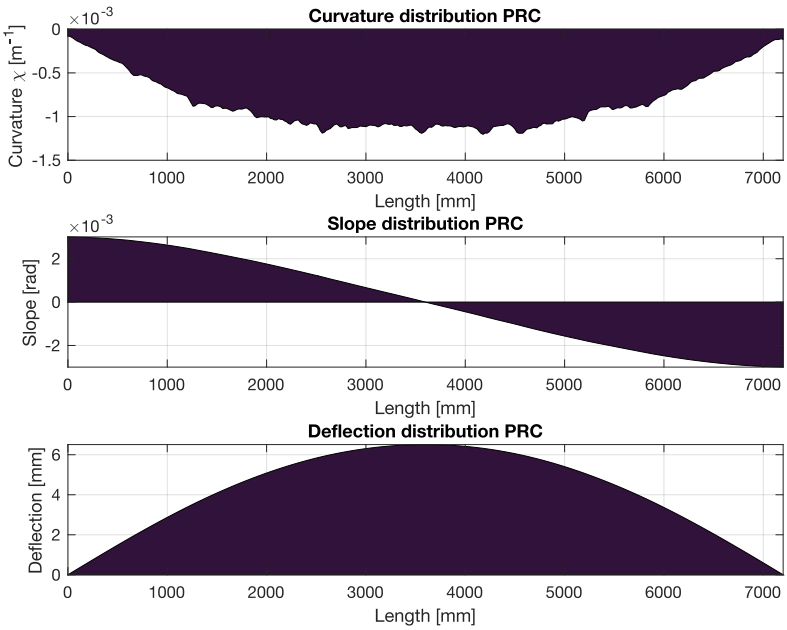

Figure 3. the calculated deflection and curvature directly after post-tensioning

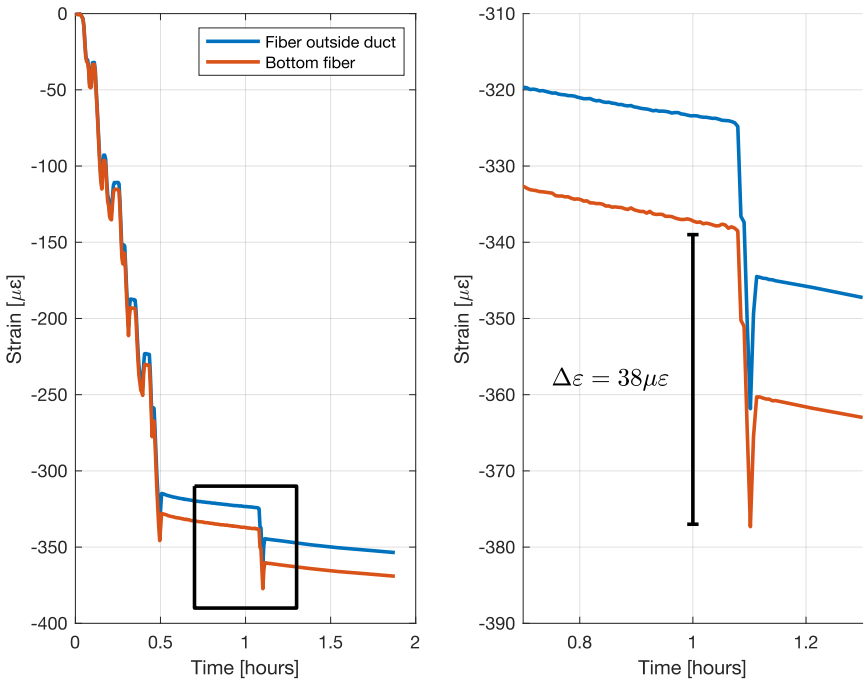

Figure 4. Looking at a small-time interval during the tensioning procedure of the PRC specimen, an interesting phenomenon can be traced. From the outside-duct strains and bottom-fibre strains, the concrete behaviour from anchor slip can be observed at the middle section of the beam.

The bending moment distribution was calculated by multiplying the curvature χ by the sectional rigidity EI. By comparing the moment distribution to the eccentricity of the prestressing steel, seen in Figure 5, it was found that the two graphs had the same shape, implying that the prestressing force, calculated by dividing the moment by the eccentricity, were more or less constant over the length of the specimen. Due to uncertainties of the tendon eccentricity in the inclined parts, only the mean prestressing force of the middle section, between the point loads, was calculated. In reality, the tendon profile had a third-degree polynomial shape, as the slope of the duct was zero both at the middle section, and in both ends due to the configuration of the anchorage.

By calculating the mean value of the prestressing force in the middle section for every time step during the post-tensioning, the prestressing force variation could be visualized. As seen in Figure 6, the different phases of the tensioning could be interpreted, as the tendons were tensioned after each other. Just as in Figure 4, the anchor slip can now be seen and magnified in the form of a force loss that directly corresponds to the force loss in the prestressing steel for the middle section.

The relation between the prestressing force at middle section compared to the active end induces that a reduction of prestressing force is present in the specimen, just as in theory. In Figure 7, the total force variation along the beam is visualized, both before and after the release of the jack. At the passive end, the prestressing force is assumed to have the same decrease of force as in the active end, due to the symmetry of the duct profile. It can also be seen that the anchor slip affects the prestressing force, causing a decrease of force from the active end to the passive end of the specimen. What is interesting from this graph is that the intersection of the two curves occur just before the end of the examined span. This indicates that the distance where anchor slip affects the prestressing force, xs, is almost as long as the examined span. The prestressing force after the intersection is unaffected by the anchor slip, meaning that it follows the same force as before the release

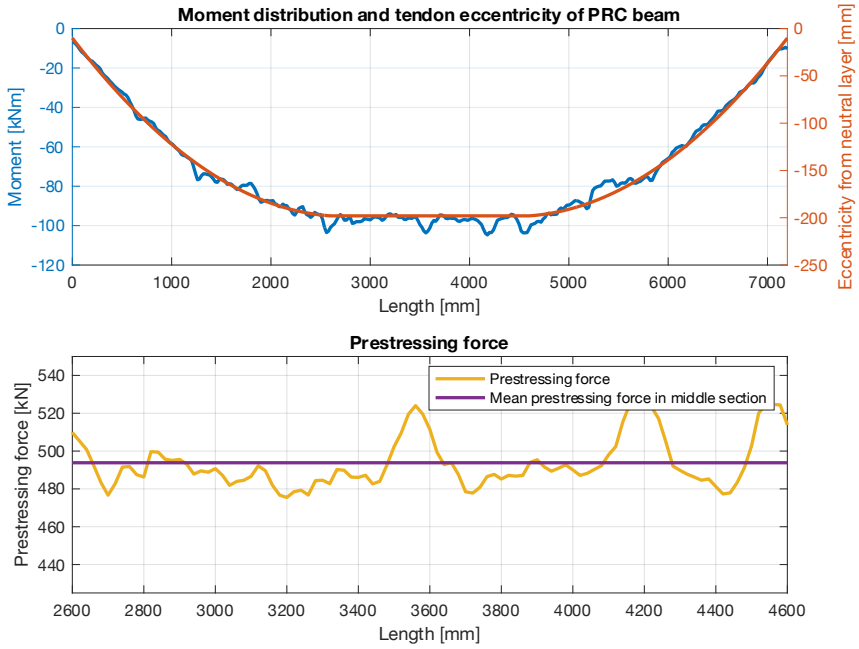

Figure 5. Bending moment distribution and prestressing force.

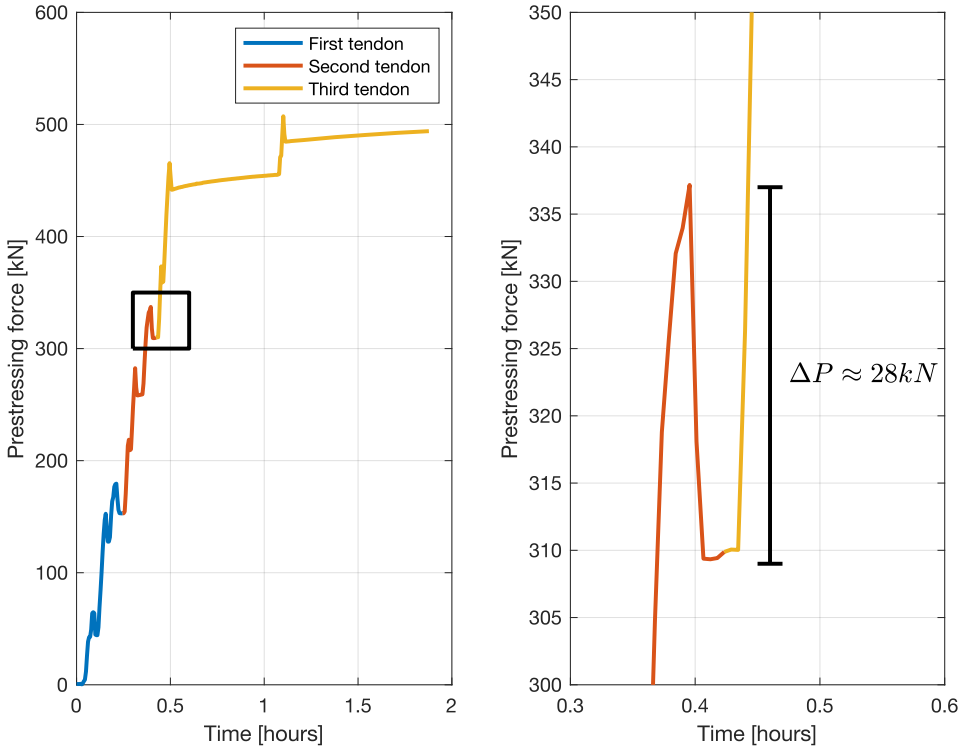

Figure 6 Phases of the tensioning

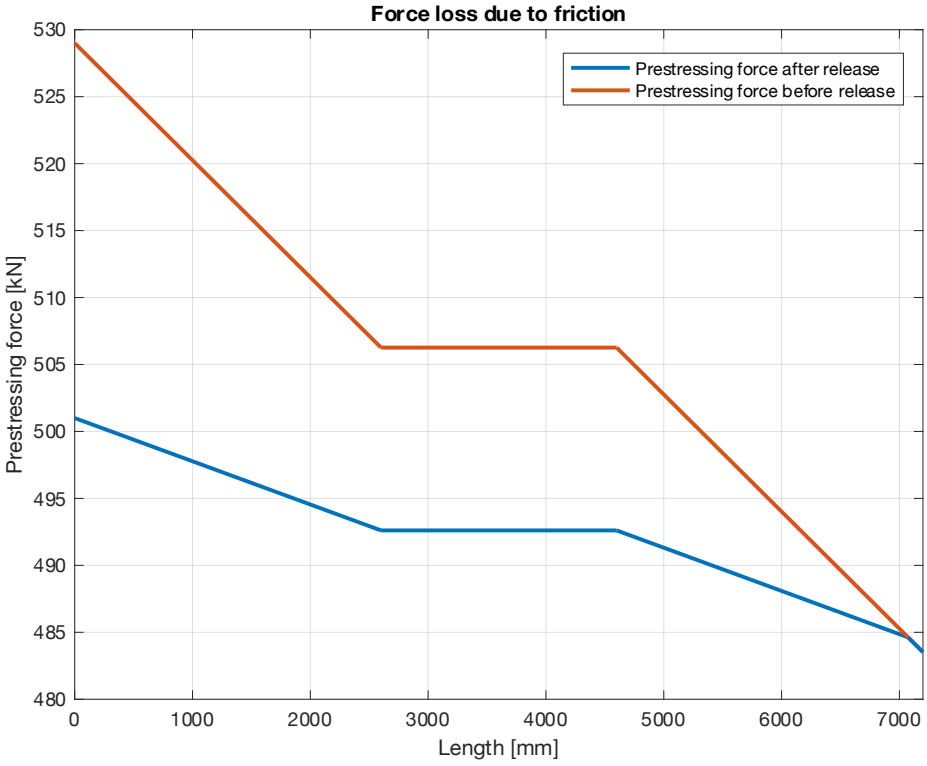

Figure 7 Total force variation along the beam.

4.1 Observations after tensioning

By keeping the specimens in an enclosed environment over time, it was possible to measure long-term effects of the two specimens. In Figure 8, the strain variation over time is visualized. The dark blue colour symbolizes the time between start and stop of the post-tensioning. Obviously, this was only the case for the PRC specimen. For both specimens, it can be interpreted that the compression is constantly increasing, which is an effect of mainly shrinkage. Notice that the strain distribution in the top fibre of the PRC specimen changes from tension to compression. For the PRC specimen, there is a rapid increase of compression during the first days, to later on have a slight decrease of contraction. For the reference specimen, the contraction is more or less constant through the time span. Looking at the change of shape, the PRC specimen has an unchanged shape, while the reference specimen curves in the top and bottom edge. The top edge will experience the largest compressive strains, as the beam is simply supported. In contrary, the bottom edge will experience the smallest compressive forces. This indicates that the long-term effects cause an increasing deflection over time. the deflection increases for the reference specimen, according to Figure 8. Looking at the PRC specimen, the curvature, slope and deflection continues to increase due to long-term effects.

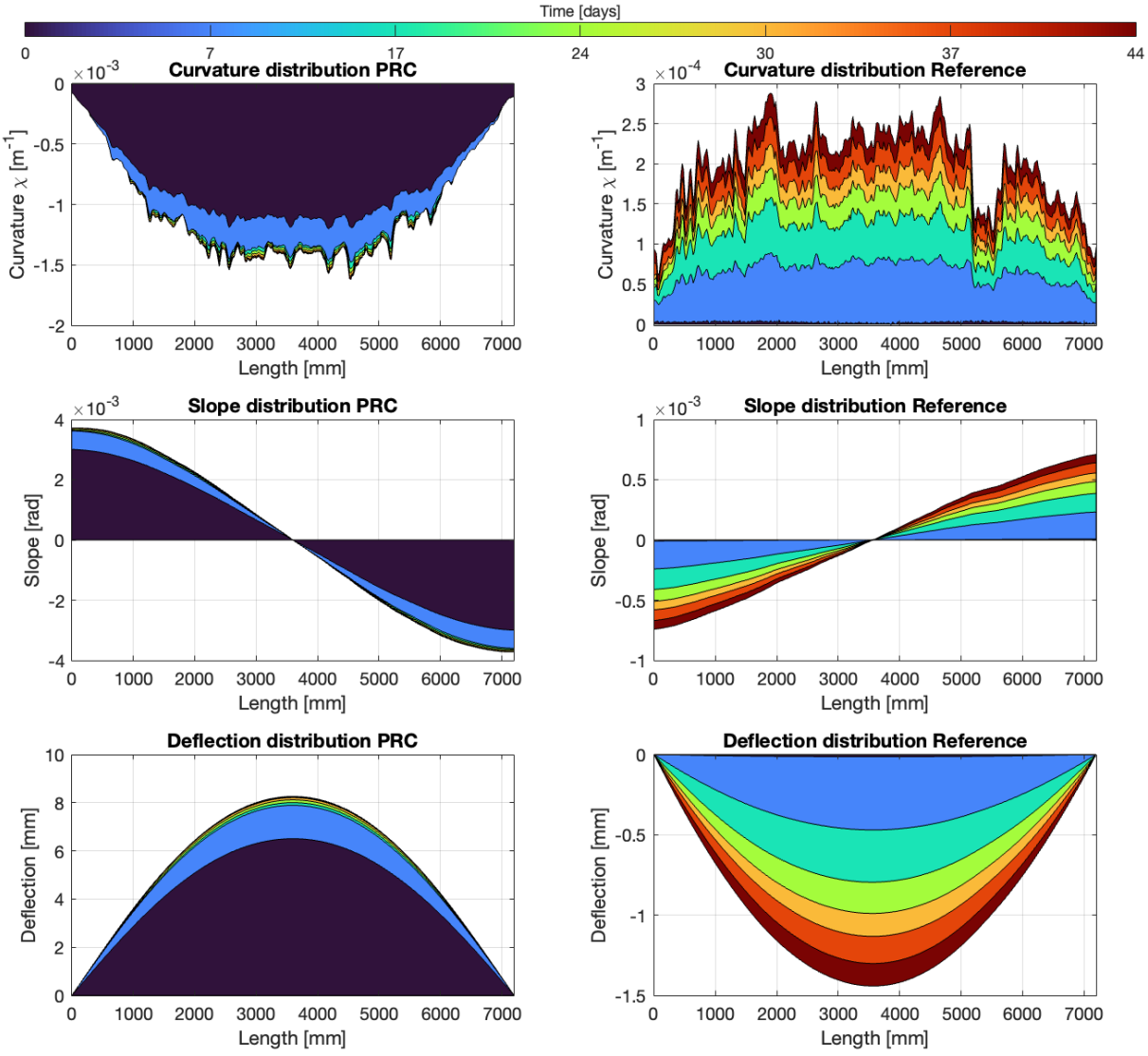

Figure 8 Long-term effects over time.

5 Conclusion

In conclusion, this project studies the usage of distributed optical fibre sensors, for further possibilities of measuring behaviour and key-performance indicators for a post-tensioned reinforced concrete beam. By using an additional reference beam, the effects of prestressing could be determined accurately by removing effects related to solely concrete, such as shrinkage and creep from self-weight. Regarding the strain from the DOFS, the quality of the output was successful. Previous research has solely tested the usage of DOFS for reinforced concrete specimens. The findings show that the usage of DOFS is feasible for post-tensioned reinforced concrete members. By com-paring results from DOFS to theoretical calculation methods, some conclusions were made. Starting with the loss of prestressing force, shrinkage and creep from self-weight was removed and only mechanical creep and relaxation was considered. The results were verified by comparing to theoretical creep and relaxation calculations. The theoretical result was on the safe side compared to result from the DOFS and might be a reason to the overestimation.

Moving on to force loss along the specimen due to anchor slip and friction, the results were similar. By comparing loss of prestressing force in the active end and middle section, a relation between loss of prestressing force over the specimen could be assessed. It was seen that the anchor slip almost affected the whole length of the specimen.

6 Acknowledgements

The main part of the experimental work was conducted in the concrete laboratory at Chalmers and the whole project was executed as a cooperation between Chalmers, WSP Sweden and NCC AB.

7 References

[1] Engström, B.: Design and analysis of prestressed concrete structures. Chalmers University of Technology, Department of Civil and Environmental Engineering, Structural Engineering, Concrete Structures, Report 2011:7, Gothenburg, 2011.

[2] H. R. Dolan, Charles W. Hamilton, Prestressed Concrete : Building, Design, and Construction. Cham, Switzerland: Springer International Publishing, 2019.

[3] B. S. Choo, “25 - reinforced and prestressed concrete,” in Advanced Concrete Technology (J. Newman and B. S. Choo, eds.), pp. 3–17, Oxford: Butterworth-Heinemann, 2003.

[4] Berrocal, C. G., Fernandez, I., Bado, M. F., Casas, J. R. , Rempling, R. “Assessment and visualization of performance indicators of reinforced concrete beams by dis-tributed optical fibre sensing,” Structural Health Monitoring, vol. 20, pp. 3309–3326, Jan. 2021.

[5] B. Glišić, D. Hubbell, D. H. Sigurdardottir, and Y. Yao, “Damage detection and characterization using long-gauge and distributed fiber optic sensors,” Optical Engineering, vol. 52, no. 8, 2013.

[6] P. Lu, N. Lalam, M. Badar, B. Liu, B. T. Chorpening, M. P. Buric, and P. R. Ohodnicki, “Distributed optical fiber sensing: Review and perspective,” Applied Physics Reviews, vol. 6, no. 4, 2019.

[7] Berrocal, I. Fernandez, and R. Rempling, “Crack monitoring in reinforced concrete beams by distributed optical fiber sensors,” Structure and Infrastructure Engineering, vol. 17, no. 1, pp. 124–139, 2021.

[8] European Committee for Standardisation, European Standard, EN 12390-3. Testing hardened concrete – Part 3: Compressive strength of test specimens. Brussel, June 2019.